Talanta 108 (2013) 53–58

Contents lists available at SciVerse ScienceDirect

Talanta

journal homepage: www.elsevier.com/locate/talanta

LIBS analysis of artificial calcified tissues matrices

M.A. Kasem [a], J.J. Gonzalez [b], R.E. Russo [b], M.A. Harith [a,*]

[a] National Institute of Laser Enhanced Science (NILES), Cairo University, Giza, Egypt
[b] Lawrence Berkeley National Laboratory, Berkeley, CA 94720, United States

ARTICLE INFO

Article history:
Received 3 January 2013
Received in revised form
25 February 2013
Accepted 26 February 2013
Available online 7 March 2013

Keywords:
UV-LIBS
Calibration
Stark broadening
Bone ash
Hydroxyapatite

ABSTRACT

In most laser-based analytical methods, the reproducibility of quantitative measurements strongly depends on maintaining uniform and stable experimental conditions. For LIBS analysis this means that for accurate estimation of elemental concentration, using the calibration curves obtained from reference samples, the plasma parameters have to be kept as constant as possible. In addition, calcified tissues such as bone are normally less "tough" in their texture than many samples, especially metals. Thus, the ablation process could change the sample morphological features rapidly, and result in poor reproducibility statistics. In the present work, three artificial reference sample sets have been fabricated. These samples represent three different calcium based matrices, $CaCO_3$ matrix, bone ash matrix and Ca hydroxyapatite matrix. A comparative study of UV (266 nm) and IR (1064 nm) LIBS for these three sets of samples has been performed under similar experimental conditions for the two systems (laser energy, spot size, repetition rate, irradiance, etc.) to examine the wavelength effect. The analytical results demonstrated that UV-LIBS has improved reproducibility, precision, stable plasma conditions, better linear fitting, and the reduction of matrix effects. Bone ash could be used as a suitable standard reference material for calcified tissue calibration using LIBS with a 266 nm excitation wavelength.

1. Introduction

1.1. Bone elemental analysis

Bone is composed of organic and inorganic matter, the inorganic matter is mainly a carbonate-containing hydroxyapatite (HAP) analog with a composition approximating $Ca_{10}(PO_4)_6(OH)_2$, also called bioapatite. HAP crystals are plate-like in morphology and have dimensions of approximately 35 nm × 5 nm with a thickness of about 2–3 nm [1]. Study of the elemental composition of bone has been used in the fields of archeology and anthropology for investigating the relationships between nutrition and diseases and to estimate the health effects of trace element deficiencies or excesses in human tissues. In addition, such studies are crucial in the verification of dietary habits [2], cultural, customs, and environmental levels of trace elements in soil and water [3]. Elemental analysis of bone also has been used to investigate toxic pollutants for example lead (Pb) exposure in historical populations or to explore the source of specific nutritional deficiencies among ancient communities [4]. These investigations depend mainly on the fact that once elements are incorporated in the hydroxyapatite structure of the bone and/or tooth matrix, a number of such elements leach out very slowly [5].

1.2. LIBS of biological samples

Laser induced breakdown spectroscopy (LIBS) has emerged as a very promising technique for the analysis and characterization of a broad variety of objects due to advantages such as: no need for laborious sample preparation, fast analysis and in-situ analysis capability. Laser ablation based analysis requires less amount of sample compared to sample digestion in conventional techniques (e.g. ICP, AAS, etc.) [6]. Typically laser ablation analysis requires femtograms to nanograms of materials compared to micrograms to milligrams for the other methods. High resolved spatial information is attainable as oppose to the complete loss of this type of information when traditional sample preparation like acidic dissolution is used. LIBS has been successfully used in the characterization of archeological bone samples from different historic ancient Egyptian dynasties in comparison with recent bone samples and it was shown that diagenesis or postmortem effects must be taken into consideration on studying dietary habits and/or toxicity levels via analysis of ancient bones [7]. In exploiting LIBS for the analysis of relatively soft biological samples such as bones,

* Corresponding author. Tel./fax: +20 23567 5335.
E-mail addresses: mharithm@niles.edu.eg, mharithm@hotmail.com (M.A. Harith).

0039-9140/$ - see front matter © 2013 Elsevier B.V. All rights reserved.
http://dx.doi.org/10.1016/j.talanta.2013.02.062

it should be taken into consideration that fast changes taking place in the target morphological features can affect the reproducibility of the results. In general biological samples are rather inhomogeneous, again influencing selectivity, statistics and reproducibility of results. To obtain reliable quantitative results using laser ablation, the experimental conditions should be maintained uniform and stable, similar to all analytical measurement technologies. For LIBS analysis this means that for accurate estimation of element concentrations, using relevant calibration curves, the plasma parameters have to be kept constant throughout the measurements [8]. For relatively soft matrices like calcified tissues this is even more important than for metallic samples. However, this is not always straight forward since drilling into the sample during repetitive single-position exposure is accompanied by a gradual change in plasma conditions. In general, a compromise has to be found in keeping the plasma conditions reasonably constant on the one hand but sampling over a sufficient number of laser pulses for statistical averaging on the other hand. At the same time, maintaining spatial resolution, if required, should be kept under control. Another difficulty in the analysis of calcified tissue samples is that suitable reference standards, required for quantification, may not be available. Quantitative analysis of trace element concentrations in calcified tissues using reference samples with a $CaCO_3$ based matrix were investigated by Samek et al. [9]. The overall physical properties of pellets pressed from $CaCO_3$ are roughly comparable to those of hydroxyapatite, but slightly more brittle than biological specimens because of the absence of the biological growth mechanism. In addition, introducing phosphorus-carrying compound was not possible because of homogeneity problems and substantial local variations in the Ca and P distribution. Also, samples based on a $CaCO_3$ matrix have shown dependence of LIBS spectra on the water content in the pellets, and it is essential to account for the water content to achieve accurate quantitative LIBS analytical results [10]. Since calcium represents the major element in the bone matrix with the highest elemental concentration, it has been used in many studies as internal standard for the calibration of elements such as Pb, Al and Sr [9]. In the present study, we had focused on studying calcium in different matrices using conventional LIBS arrangement at two different excitation wavelengths, 1064 nm and 266 nm to examine the stability of plasma conditions in different matrices, measure the extent of matrix effects, and the reproducibility and precision for calibration.

2. Methodology

2.1. Samples

Three sets of reference samples representing three different calcium based matrices have been fabricated. Each sample was mixed with paraffin binder for 10 min using an automatic mixer machine (Spex Sample Prep, Mixer/Mill 8000M) and then pressed into a pellet using an automatic press (Spex Sample Prep, X-press 3630). The samples were pressed into pellets using an automatic program to assure reproducibility set at 25 t of pressure for 1 min for 5 g pellet, and 7 t of pressure for 2 min for 1 g pellet. The 1st sample set was a calcium carbonate matrix; 10 samples were prepared by mixing pure powder of $CaCO_3$ with different amounts (by weight) of $MgCO_3$ and paraffin (binder). Samples with a calcium concentration in the range of 0.1–10% were obtained while the Mg content was fixed at 1%. The 2nd set was a hydroxyapatite matrix; 7 samples were prepared using a similar procedure but this time by mixing the paraffin with high purity powder of Ca-Hydroxyapatite "solid dilutions" calcium concentration was set in the range 1–9%. Ca-Hydroxyapatite was obtained from the National Institute of Standards and Technologies (NIST2910). It is a high purity powder formed of crystalline calcium hydroxyapatites of about 0.1–0.5 μm sizes. One unit of SRM2910 consists of 2 g of material synthesized at the NIST by solution reaction of calcium oxide and phosphoric acid. It has certified values (Ca 39.15%, P 18.18%, Ca/p 2.15) and reference values (hydrogen phosphate 0.592%, carbonate content 0.032%, water content 1.5%) and is used to simulate the molecular structure of bone apatite. Lastly, the 3rd set was of bone ash matrix; 8 samples were prepared using the same procedure by mixing the paraffin with the high purity powder bone ash "solid dilutions" calcium concentration was set in the range 1–10%. Bone ash was obtained from the National Institute of Standards and Technologies (NIST 1400). It consists of bone ash that was blended to a high degree of homogeneity. It has certified values (Ca 38.18%, P 17.9%, Mg 0.68%, Sr 249 μg/g, Fe 660 μg/g, Pb 9.07 μg/g, K 186 μg/g, Zn 181 μg/g) and non-certified concentrations (Si 0.13%, Na 0.6%, Al 530 μg/g, Ar 0.4 μg/g, Cd 0.03%, Cu 2.3%, F 1250 μg/g, Mn 17 μg/g, Se 0.08%).

2.2. LIBS arrangements

Two LIBS experimental systems based on an RT100 design (Applied Spectra, Inc.) with different laser excitation wavelengths (1064 nm, 266 nm) were used throughout the measurements. The experimental conditions (laser energy, spot size, repetition rate, irradiance, etc.) for the two systems (Table 1) were kept as close as possible to investigate the wavelength effect.

In the 1st setup the laser source was a Q-switched Nd:YAG laser (New wave, Minilase II, USA), operating at its fundamental wavelength ($\lambda = 1064$ nm), with a pulse duration of 6–8 ns. The pulse energy was set to 22 mJ and the repetition rate to 5 Hz. The laser beam was tightly focused vertically onto the target surface using an objective lens (LmH-5x-1064, Thorlab, USA). High resolution camera (USB 2.0 CMOS Camera, Thorlab, USA) was used for viewing the sample surface and adjusting the laser focus. The samples were mounted on an *X*–*Y*–*Z* motorized translational stage. LIBS spectra were collected from 10 replicates from fresh spots, 100 accumulative shots were recorded for each spot to optimize the signal-to-noise ratio and establish reproducibility.

The plasma optical emission was collected through a plano-convex lens with 4 cm focal length to fiber-optics bundle for light coupling to the spectrometer entrance slit. The spectrometer (LIBS Aurora spectrometer, 6 channel CCD, Applied spectra, Inc., USA) covers the spectral coverage (190–1040 nm), with spectral resolution < 0.1 nm for UV to VIS, and < 0.12 nm for VIS to NIR. The detector type was a CCD linear array; the spectrometer gating control is achieved through fully integrated electronic pulse generator gate delay adjustment from 50 ns to 10^6 ns with 25 ns step resolution, with integration time 1.04 ms–10^4 ms. To obtain the optimum delay time an optimization procedure has been performed where the delay time has been changed in steps

Table 1
LIBS measurement parameters.

Experimental parameters	LIBS-1064 nm	LIBS-266 nm
Wavelength (nm)	1064	266
Pulse width (ns)	~7	~5
Energy (mJ)	~22	~14.3
Laser repetition rate (Hz)	5	5
Number of shots	100	100
Irradiance (W/cm^2)	1.778×10^{10}	2.154×10^{10}
Fluence (J/cm^2)	124	107
Replicates	10	10
Spot size diameter (μm)	~150	~130
Delay time (μs)	1	1
Integration time (ms)	1.04	1.04
Spectrometer	6-Channels CCD, Aurora	6-Channels CCD, Aurora

of 200 ns. The optimized delay time used in the present measurements was fixed at 1000 ns, with integration time 1.04 ms. The spectrometer is compatible with externally triggered Nd:YAG lasers, laser firing control (frequency and number of pulses) is achieved with integrated electronic pulse generator. Statistical monitoring of the spectral line intensities, curve-fitting of overlapping peaks, background subtraction and automatic peak integration was done using Aurora software (Applied Spectra, Inc.). In the 2nd system, the laser was (New wave, Tempest-10 Hz, USA) operating at its 4th harmonic (λ=266 nm), with a pulse duration of 3–5 ns. The pulse energy was set to 14 mJ and the repetition rate to 5 Hz. The laser beam was tightly focused vertically onto the sample surface using an objective lens (LMV-5x-UVB, Thorlab, USA) the rest of the arrangements was the same as mentioned in the 1st setup.

3. Results and discussion

3.1. LIBS spectra

Fig. 1 shows LIBS normalized spectra for three different calcium matrices (a) $CaCo_3$–1% Mg, (b) Ca-Hydroxyapatite, and (c) bone ash at the same calcium concentration 9% using excitation laser wavelengths 1064 nm and 266 nm. Spectra were normalized using the CN band emission from the paraffin binder in the sample pallets. The figure shows ionic Ca(II)-393 nm, Ca(II) 396 nm and the atomic Ca(I)-422 nm lines; the relative intensities were higher for 1064 nm than 266 nm for the carbonate matrix (Fig. 1a).

The higher intensity with 1064 nm excitation could be due to the fact that the fluence threshold of plasma formation is lower for longer wavelength as has been confirmed previously by other authors for the three wavelengths 266, 532, and 1064 nm [11]. This also agrees with the assumption of plasma ignition by inverse Bremsstrahlung, which is approximately proportional to λ^3 that makes IR more favorable than UV wavelengths for plasma heating. There is a pronounced increase of ionic emission lines intensity in case of 1064 nm compared to the intensities in case of the 266 nm excitation for all three measured matrices (Fig. 1a–c). This is mainly because the plasma generated by UV laser has lower temperature and electron density than in case of IR generated plasma [12]. It is also noticeable that the UV excited spectral lines are in general narrower in addition to their reduced intensity compared to the lines in case of IR excitation as has been reported earlier [13].

4. Stark broadening

Stark line broadening due to collisions of charged species is the primary mechanism influencing the emission spectral bandwidth in conventional LIBS experiments [14]. The (FWHM) $\Delta\lambda_{1/2}$ of Stark broadened lines and the electron number density (N_e) are

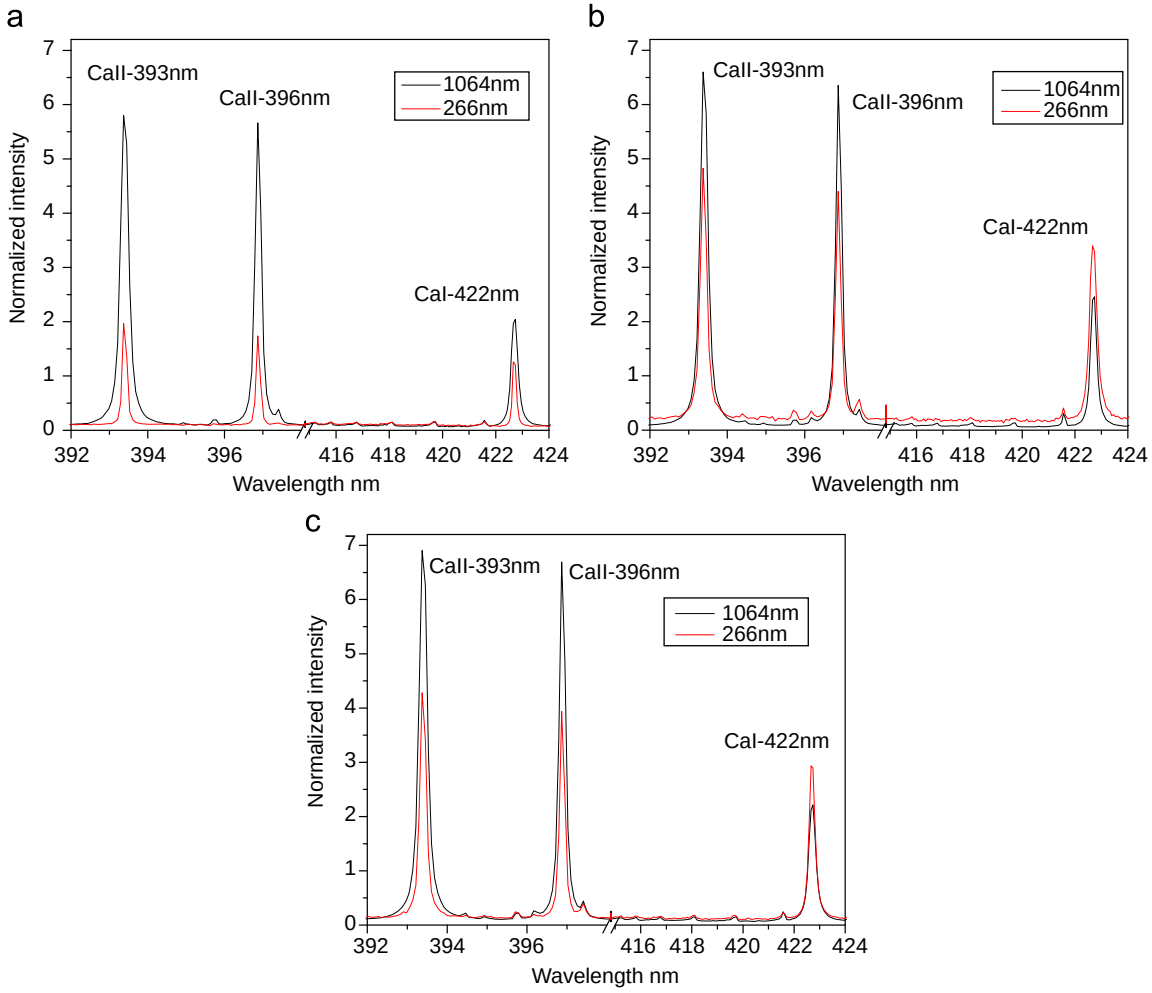

Fig. 1. LIBS normalized spectra from three matrices: (a) calcium carbonate 1%Mg, (b) calcium hydroxyapatite, and (c) bone ash, at Ca conc. 9% for two laser excitation wavelengths λ=1064 nm and 266 nm.

related by the following equation [14,15].

$$\Delta\lambda_{1/2} = 2w\left(\frac{N_e}{10^{16}}\left[1+1.75A\left(\frac{N_e}{10^{16}}\right)^{1/4}\left(1-\frac{3}{4}N_D-\frac{1}{3}\right)\right]\right) \quad (1)$$

where N_D is the number of particles in the Debye sphere and is estimated from:

$$N_D = 1.72 \times 10^9\ (T_e^{3/2})/(N_e^{1/2}) \quad (2)$$

where w is the electron impact parameter in nm and A is the ion impact parameter; both w and A are functions of temperature.

Stark line broadening for Mg in the $CaCO_3$ matrix was investigated. Fig. 2 depicts the normalized atomic line Mg(I)-285 nm at different Ca concentrations (0.1–10%) for laser excitation wavelengths 1064 nm and 266 nm. The spectral line profiles were fitted by *Lorentzian* function. It is clear from this figure that Stark line broadening of Mg(I) in case of 1064 nm laser excitation increases with increasing calcium concentration in the matrix till it reaches maximum at 8% calcium then levels off, while for 266 nm it shows narrower lines and more stable FWHM with changing Ca concentration.

The red shift in λ_{max} for 266 nm excitation results from *Lorentzian* function fitting procedure due to the asymmetry of the Mg(I) line which could be due to integration time over 1 ms. This confirms that the plasma generated by UV-laser excitation is more resistant to the matrix effect due to change of calcium concentration. This advantage is valuable for archeological bone elemental quantification where calcium, normally used as internal standard, could vary in concentration due to bone degradation or diagenesis.

Using Eq. (3) plasma temperature has been calculated using two calcium lines of same ionization $\lambda_1 = 315$ nm and $\lambda_2 = 370$ nm, while atomic temperature was calculated using calcium atomic lines at $\lambda_1 = 487.8$ nm and $\lambda_2 = 527$ nm. Ionic temperature was calculated using ionic lines

$$\frac{I_1}{I_2} = \left(\frac{\lambda_2}{\lambda_1}\right)\left(\frac{g_1}{g_2}\right)\left(\frac{A_1}{A_2}\right)e^{-(E1-E2)/KT} \quad (3)$$

where I_1, I_2 are the line intensities of same species of ionization, K (eV/K) is the Boltzmann constant, g and E (eV) are, respectively the statistical weight and excitation energy of upper level, while A

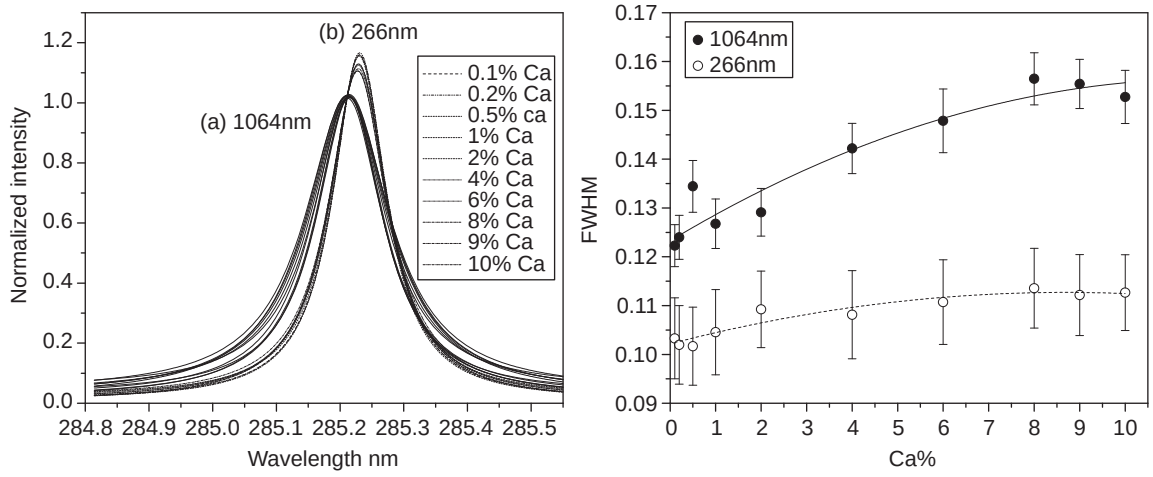

Fig. 2. Normalized atomic Mg(I)-285 nm, fitted using Lorentz peak fitting, at fixed Mg conc. 1% and varying Ca concentration (0.1–10%) for two laser excitation wavelengths 1064 nm and 266 nm.

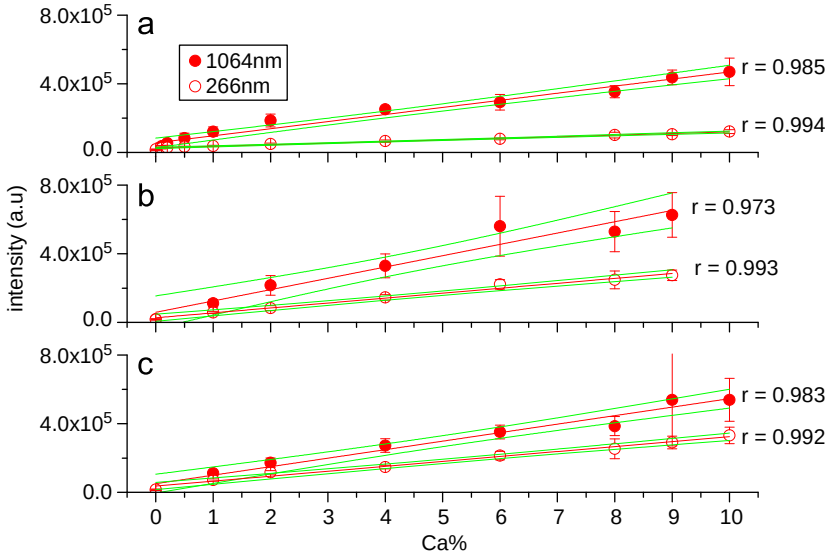

Fig. 3. Atomic line calibration for Ca (I)-422 nm for three matrices: (a) $CaCO_3$, (b) Ca-Hydroxyapatite, and (c) bone ash, for two laser excitation wavelengths $\lambda = 1064$ nm and 266 nm.

(s^{-1}) is the transition probability. For the highest calcium concentration in $CaCO_3$ matrix (10%), plasma atomic and ionic temperatures were respectively calculated as $T_{e(atom)}=7531$ K and $T_{e(ion)}=8111$ K which are very near to each other within the experimental error (10%). This indicates that LTE conditions are fulfilled.

4.1. Calibration curves

Fig. 3 shows calibration lines for Ca(I) 422 nm in the three different matrices for laser excitation wavelengths (1064 nm, 266 nm). Higher sensitivity has been obtained in case of using the 1064 nm wavelength as shown from the slope values given in Table 2, while the UV excitation at 266 nm show better linear fitting, (i.e. Pearson's correlation r) and reproducibility (i.e. standard deviation error bars). The better correlation factor (r) for UV-LIBS could be due to lower thermal effects induced at the sample surface by the UV radiation, leading to a pronounced improvement in the ablation rate [15]. Neither self-absorption nor plasma shielding show up in view of the absence of saturation in the obtained calibration curves. This may be attributed to the plasma thinness.

The confidence bands shown in the figures represent the 95% confidence limits of all possible fitted regression lines also called least square. The narrow confidence bands for the UV-266 nm LIBS means a better precision for the calibration. The confidence band for Ca-hydroxyapatite matrix (Fig. 3b) is wider than the other 2 matrices for 1064 nm-LIBS. This may be attributed to the matrix crystalline structure with crystal size (0.1–0.5 μm) that could lead to inhomogeneity in pellets whereas both $CaCO_3$ and bone ash are powder at high degree of homogeneity, the problem of inhomogeneity does not appear for UV-LIBS since it was proven in literature that UV-LIBS has better ablation rate, less thermal effect and low digging in the samples [15]. The hydroxyapatite matrix resembles bone pure crystalline structure with Ca/P=2.15, while bone ash matrix resembles bone different elements constituents in the matrix with Ca/P=2.13. These two matrices should give a complete picture for matrix matched standards for bone calibration. Fig. 3(b) and (c) show that peak integration intensity for bone ash and Ca-hydroxyapatite at 266 nm laser excitation is very similar, thus using UV-LIBS in calibration for calcified bone samples should be more appropriate.

Table 2
Slope values for atomic line calibration for Ca (I)-422 nm for $CaCO_3$, Ca-Hydroxyapatite, and Bone ash, for two laser excitation wavelengths $\lambda=1064$ nm and 266 nm.

Matrix	LIBS-1064 nm	LIBS-266 nm
$CaCO_3$	41,331.40	9337.06
Ca-Hydroxyapatite	65,922.07	28,664.36
Bone ash	49,534.53	28,725.48

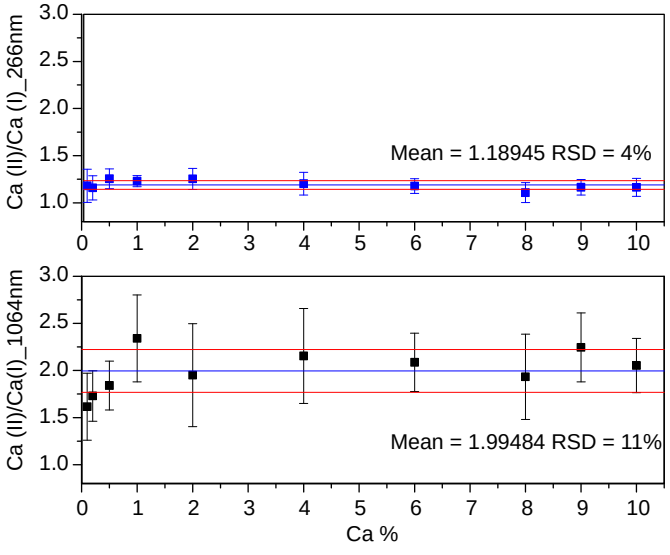

Fig. 4. $CaCO_3$ Ca (II)-393 nm/Ca(I)-422 nm ionic to atomic line ratio for two laser excitation wavelengths $\lambda=1064$ nm and 266 nm.

4.2. Plasma stability

Figs. 4–6 show the ionic to atomic line ratio of two Calcium lines Ca(II)-393 nm/Ca(I)-422 nm in the three different matrices

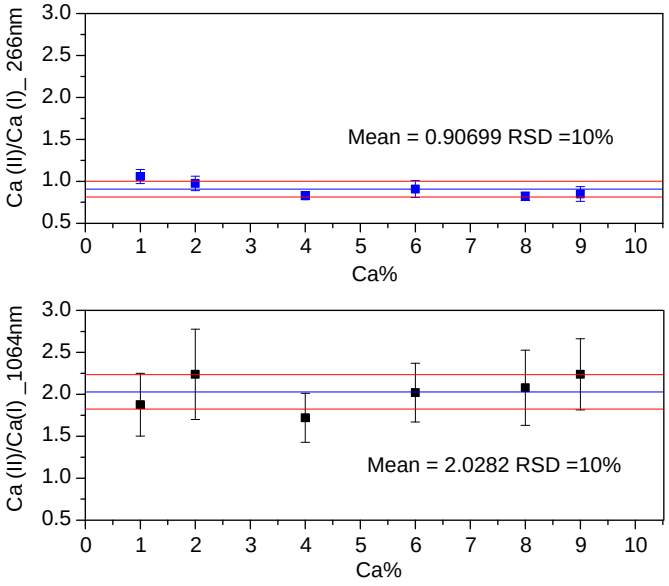

Fig. 5. Ca-Hydroxyapatite Ca(II)-393 nm/Ca(I)-422 nm ionic to atomic line ratio for two laser excitation wavelengths $\lambda=1064$ nm and 266 nm.

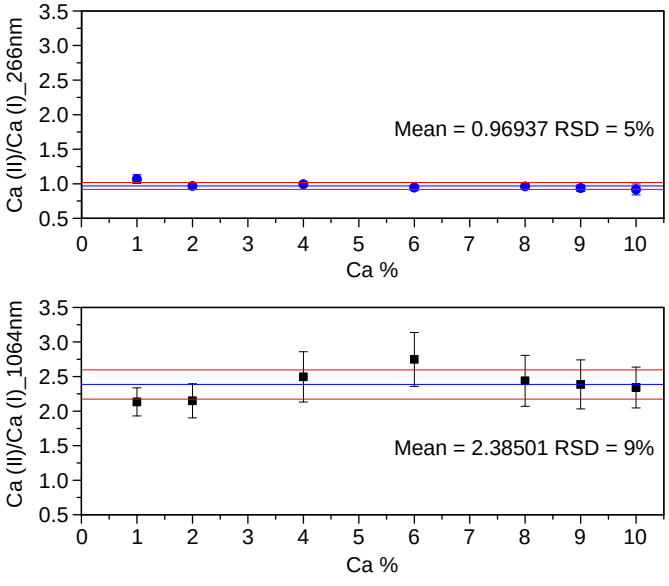

Fig. 6. Bone ash Ca (II)-393 nm/Ca(I)-422 nm ionic to atomic line ratio for two laser excitation wavelengths $\lambda=1064$ nm and 266 nm.

at the two laser excitation wavelengths (λ=1064 nm, 266 nm). The figures depict the plasma stability from ionic to atomic line ratios (CaII/CaI) as calcium concentration changes.

UV-LIBS shows that plasma stoichiometry (CaII/CaI) is more stable with changing calcium concentration i.e. relative standard deviation (RSD), and it has better reproducibility i.e. error bars. This can be interpreted in view of the fact that shorter wavelengths offer higher photon energies for bond breaking and ionization processes, the UV wavelength 266 nm has photon energy of 4.7 eV compared to 1064 nm that provides 1.16 eV [16]. For most materials, bonding energy is a few eV, when the photon energy is higher than the bond energy, photon-ionization occurs and non-thermal mechanisms will play an important role in the ablation process. In addition, shorter optical penetration depth exists with UV-wavelengths, providing more laser energy per unit volume for ablation. In general better plasma stoichiometry is achieved with UV excitation due to the reduced matrix effect. Longer wavelengths on the other hand favor the inverse Bremsstrahlung plasma shielding processes, but lower the ablation rate and increase the chances of elemental fractionation [17]. Russo et al. [18] studied the influence of laser wavelength on fractionation in laser ablation by comparing three different UV wavelengths (266 nm, 213 nm and 157 nm). It was found that the shorter the wavelength, the more controlled and reproducible was the ablation rate.

5. Conclusions

- These studies demonstrate that UV-LIBS for calibration of prepared reference samples resembling bone calcified tissue provide higher reproducibility, better linear fitting, and stable plasma conditions than IR-LIBS.
- UV-LIBS showed reduced dependency to changes in Ca concentration (matrix effects) as shown from the results of the stark broadening of Mg (I) line.
- Bone ash could be the most suitable standard reference material for calcified tissue calibration in case we use LIBS at 266 nm excitation wavelength.

Acknowledgment

RER and JJG acknowledge support by the Chemical Science Division, Office of Basic Energy Sciences of the U.S. Department of Energy under contract number DE-AC02-05CH11231 at the Lawrence Berkeley National Laboratory

References

[1] H.A. Lowenstam, S. Weiner, Biomineralization, Oxford University Press, Oxford, 1989.
[2] Louise T. Humphrey, M. Christopher Dean, Teresa E. Jeffries, Malcolm Penn, PNAS 105 (2008) 6834–6839.
[3] P. Budd, J. Montgomery, A. Cox, P. Krause, B. Barreiro, R.G. Thomas, Sci. Total Environ. 220 (1998) 21–36.
[4] K.C. Stamoulis, P.A. Assimakopoulos, K.G. Ioannides, E. Johnson, P.N. Soucacos, Sci. Total Environ. 229 (1999) 165–182.
[5] H.S. Vuorinen, S. Pihlman, H. Mussalo-Rauhamaa, U. Tapper, T. Varrela, Sci. Total Environ. 177 (1996) 145–160.
[6] D.W. Hahn, N. Omenetto, Appl. Spectrosc. 64 (2012) 347–419.
[7] A. Kasem, E. Russo, Mohamed Abdel Harith, J. Anal. At. Spectrom. 26 (2011) 1733–1739.
[8] Z.A. Abdel-Salam, Z. Nanjing, D. Anglos, M.A. Harith, Appl. Phys. B 94 (2009) 141–147.
[9] O. Samek, D.C.S. Beddows, H.H. Telle, J. Kaiser, M. Liška, J.O. Cáceres, A. Gonzáles Ureña, Spectrochim. Acta B 56 (2001) 865–875.
[10] D.A. Rusak, M. Clara, E.E. Austin, K. Visser, R. Niessner, B.W. Smith, J.D. Winefordner, Appl. Spectrosc. 51 (1997) 1628–1631.
[11] L.M. Cabalin, J. Laserna, Spectrochim. Acta B 53 (1998) 723–730.
[12] F. Dahmani, Phys. Fluids B: Plasma Phys. 4 (1992) 1943–1952.
[13] Y.-I. Lee, K. Song, H.-K. Cha, J.-M. Lee, M.-C. Park, G.-H. Lee, J. Sneddon, Appl. Spectrosc. 51 (1997) 959–964.
[14] H.C. Liu, X.L. Mao, J.H. Yoo, R.E. Russo, Spectrochim. Acta B 54 (1999) 1607–1624.
[15] R. Fantoni, L. Caneve, F. Colao, L. Fornarini, V. Lazic, V. Spizzichino, in: B. DiBartolo, O. Forte (Eds.), Advances in Spectroscopy for Lasers and Sensing, Springer, New York, 2006, pp. 229–254.
[16] X.L. Mao, W.T. Chan, M.A. Shannon, R.E. Russo, J. Appl. Phys. 74 (1993) 4915–4922.
[17] R.E. Russo, X.L. Mao, J. Yoo, J.J. Gonzalez, Laser Induced Breakdown Spectroscopy, in: S.N. Thakura, J.P. Singh (Eds.), Laser ablation, Elsevier, 2007, pp. 49–82.
[18] R.E. Russo, X.L. Mao, O.V. Borisov, H.C. Liu, J. Anal. At. Spectrom. 15 (2000) 1115–1120.